

Imaging and burst location with the EXIST high-energy telescope

Gerald K. Skinner^{a,b}, Scott Barthelmy^c, Mark H. Finger^d, Jae Sub Hong^e, Garrett Jernigan^f, Stephen J. Sturmer^{a,g}, Branden T. Allen^e and Jonathan E. Grindlay^e

^a CRESST & NASA-GSFC, Greenbelt, MD 20771, USA;

^b Department of Astronomy, Univ. Md., College Park, MD 20742, USA;

^c NASA-GSFC, Greenbelt, MD 20771, USA;

^d USRA & NASA-MSFC, Huntsville, AL 35812, USA;

^e Harvard-Smithsonian Center for Astrophysics, 60 Garden St., Cambridge, MA 02138 USA;

^f Space Science Lab., UCB, Berkeley, CA 94720, USA;

^g Univ. Md. Baltimore County, USA

ABSTRACT

The primary instrument of the proposed EXIST mission is a coded mask high energy telescope (the HET), that must have a wide field of view and extremely good sensitivity. In order to achieve the performance goals it will be crucial to minimize systematic errors so that even for very long total integration times the imaging performance is close to the statistical photon limit. There is also a requirement to be able to reconstruct images on-board in near real time in order to detect and localize gamma-ray bursts, as is currently being done by the BAT instrument on Swift. However for EXIST this must be done while the spacecraft is continuously scanning the sky. The scanning provides all-sky coverage and is also a key part of the strategy to reduce systematic errors. The on-board computational problem is made even more challenging for EXIST by the very large number of detector pixels (more than 10^7 , compared with 32768 for BAT). The EXIST HET Imaging Technical Working Group has investigated and compared numerous alternative designs for the HET. The selected baseline concept meets all of the scientific requirements, while being compatible with spacecraft and launch constraints and with those imposed by the infra-red and soft X-ray telescopes that constitute the other key parts of the payload. The approach adopted depends on a unique coded mask with two spatial scales. Coarse elements in the mask are effective over the entire energy band of the instrument and are used to initially locate gamma-ray bursts. A finer mask component provides the good angular resolution needed to refine the burst position and reduces the cosmic X-ray background; it is optimized for operation at low energies and becomes transparent in the upper part of the energy band where an open fraction of 50% is optimal. Monte Carlo simulations and analytic analysis techniques have been used to demonstrate the capabilities of the proposed design and of the two-step burst localization procedure.

Keywords: X-ray imaging, Gamma-ray imaging, Gamma-ray bursts, EXIST

1. INTRODUCTION

The Energetic X-ray Imaging Survey Telescope (EXIST) mission¹ is optimized for study of Gamma-Ray Bursts (GRBs) as probes of the high- z Universe^{2,3} but will also contribute to a wide range of other science (*e.g.* Refs. 4–6) by conducting a sky-survey in the hard X-ray /soft gamma-ray bands. The main instrument, the high energy telescope (HET)⁷ is a coded-mask telescope operating in the band 5–600 keV and has a very wide field of view – 1.2 sr at any instant (to 10% effective area), extended by continuous scanning. It is complemented by narrow field X-ray and optical/infrared instruments, the SXI covering 0.1–10 keV⁸ and the IRT (0.2–2.2 μm).⁹

The GRB and sky-survey aspects of the mission each present important challenges related to the associated HET image reconstruction and processing. For the GRB observations images must be reconstructed on board in very close to real time in order to detect the appearance of GRBs or new transient sources and to automatically

Send correspondence to G.K.S: E-mail: skinner@milkyway.gsfc.nasa.gov

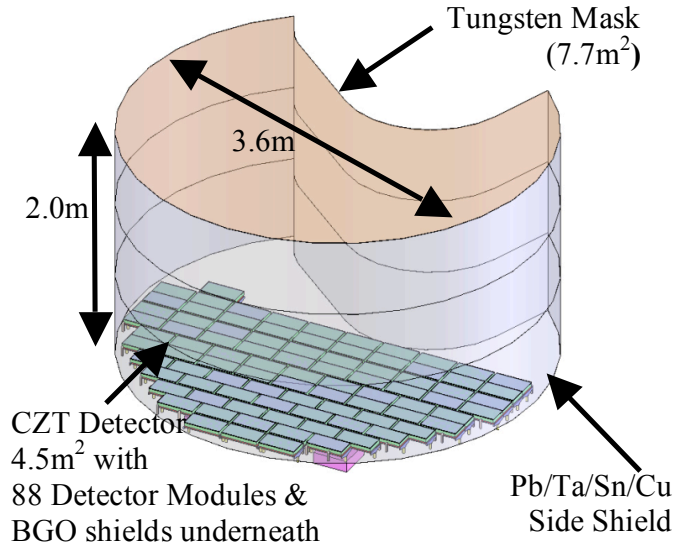


Figure 1. The basic layout of the EXIST HET coded mask instrument.

initiate a slew to bring the location of the detected event within the field of view of the narrow-field instruments. The 2 year survey phase of the 5 year mission will involve combining large amounts of data together, and it is important that systematic effects are kept to an absolute minimum to avoid them becoming a dominant source of uncertainty when the Poisson noise is reduced to a very low level.

The EXIST HET Imaging Technical Working Group, of which the authors of this paper are members, investigated and compared numerous alternative designs for the HET. We discuss here the issues considered and how image processing requirements and imaging-mode sensitivity influenced the choice of adopted design.

2. THE HET IMAGING DESIGN AND THE LOGIC BEHIND IT

Although numerous alternatives have been considered and assessed, the concept adopted for the HET is a very simple one – a plane coded mask is supported 2 m above a plane detector array and parallel to it. The mask is as large (7.7 m^2) as possible within the constraints of the launch vehicle shroud and other instruments. The detector array is almost as large, though limited to 4.5 m^2 of useful geometric area by practical considerations (required space between modules, complexity, and mass). Similarly, the detector pixel size ($0.6 \text{ mm} \times 0.6 \text{ mm}$) as small as practical considerations permit.

In many of the instrument concepts considered but not finally adopted, the mask and/or detector were divided into sub-units, angled differently in an attempt to obtain an even larger field of view. At one extreme (Fig. 2a) such designs may have entirely independent subunits, with different fields of view and with shielding walls such that radiation entering through the mask of one unit cannot reach the detector of another. At the other extreme a single multi-faceted mask may cast shadows onto an array of detector sub-units, oriented so as to view predominantly in different directions (e.g. the wide field instrument in Fig. 2b).

It was found that designs with multiple independent sub-telescopes suffered a weight penalty because of all the shielding and did not reap the full benefits of the coded mask technique, which offers the largest multiplex advantage when the field of view is as wide as possible.

The difficulty with designs with ‘shared’ masks is less obvious. and is entirely associated with practicability of data analysis. Image reconstruction from coded mask telescope data is basically a matter of correlation of the pattern recorded in the detector plane with that expected from trial source positions in each pixel in the sky image. With millions of detector pixels and millions of image pixels, this is potentially a huge problem. With a classical coded mask telescope, such as the narrow field instruments in Fig. 2b, the shadow cast on the detector by sources in different directions within the field of view are simply shifts of that from an on-axis source.

Thus all the correlations to be performed are those between the recorded data pattern and different shifts of a representation of the mask pattern. As will be discussed below, this is a process that can be performed very efficiently by a Fast Fourier Transform (FFT). However, if the mask and detector are not plane and parallel, as in the main instrument in Fig. 2b, there is no such simple relationship between the shadows cast by sources in different directions. At best, FFTs can be used to give approximate solutions over a limited region of sky.

In principle, back-projection techniques¹⁰ allow the analysis of data from coded mask systems with arbitrary geometry and they have been proposed for designs even more extreme than some of those considered for the EXIST HET (e.g. Ref. 11). However, as will be seen below, the computational requirements for its application to the HET preclude its use for on-board imaging, though it will be seen below that it can play a valuable rôle in refining GRB locations. Thus despite the constraints that it imposes, the efficiency of the FFT is crucial and it is this that drove the EXIST design in the direction of plane parallel mask and detector planes.

Other critical parameters for the imaging design are the mask to detector separation or ‘focal length’, f , the size, m , of the mask holes and the ‘open fraction’ q of the mask. We here consider the detector pixel size d to be already fixed at a value that is as fine as is possible given available detector technology, and cost and complexity limits. For the present purposes that is taken to be 0.6 mm. The considerations that led to the choices made are:

- m The dependence of the angular resolution on m implies that it should be as small as possible, but the loss in sensitivity when the detector pixels imperfectly resolve the shadows of the holes¹² limits how far it is sensible to go in this direction. For a source detected with adequate significance, it can be shown that the choice of $m = d$ optimizes the source location accuracy,¹³ but this choice reduces the sensitivity to 2/3 of that possible with $m \gg d$ and so fewer sources will be detectable. A value of $m = 1.15$ mm has been baselined, corresponding to $m/d=1.9$ and a sensitivity factor¹² $S/S_\infty = 1 - d/3m = 83\%$ for a mask with all holes of this size. However, as will be seen below, the mask pattern adopted improves on this.
- f Given that the extent of the mask and of the detector are limited by the shroud and by other instruments, the shorter the focal length the wider the field of view. On the other hand the angular resolution at the center of the field of view is approximately $\sqrt{d^2 + m^2}/f$ and so becomes poorer for small f . The compromise adopted is $f=200$ cm.
- q Equations for the optimum value of the open fraction have been given in the literature (see 13 and references therein). Where the detector background is dominated by effects not dependent on the sky exposure (e.g. background due to high energy particles) the optimum is $q=50\%$. However where the diffuse X-ray background is important – generally at lower energies and for wide fields of view – a lower q is preferable. Lower values of q also reduce the detected event rate and hence data handling problems. The adopted design has $q \sim 0.2$ at low energy and ~ 0.5 at high.

3. IMAGING WITH A SCANNING CODED MASK TELESCOPE

The fact that for much of the mission EXIST will be scanning the sky has many advantages. For the detection of phenomena that are short-lived (but not instantaneous) the region surveyed is larger. For longer term observations the effects of most types of systematic noise are smeared out and drastically reduced. However it also makes the data analysis, particularly the on-board near-real-time analysis, more of a challenge.

For back-projection techniques there is simply the added complication that the mapping onto the sky of the mask, as seen by the detector element in which the photon is detected, is continuously changing. For correlation image reconstruction, by FFT or otherwise, the implications of scanning are more serious. Such techniques involve binning the data and the interval over which the situation can be considered static can be very short when the angular resolution is high. A separate reconstruction must be performed for each such time bin and the resulting tangent plane images with different centers must be combined. A prototype scanning coded aperture imaging analysis system has been developed for the Swift/BAT Slew Survey (BATSS) and demonstrated.¹⁵

The interval over which data may be binned can be extended somewhat using ‘Time Domain Integration’ (TDI) – taking advantage of the fact that to a first approximation the shadows of the mask cast by sources in

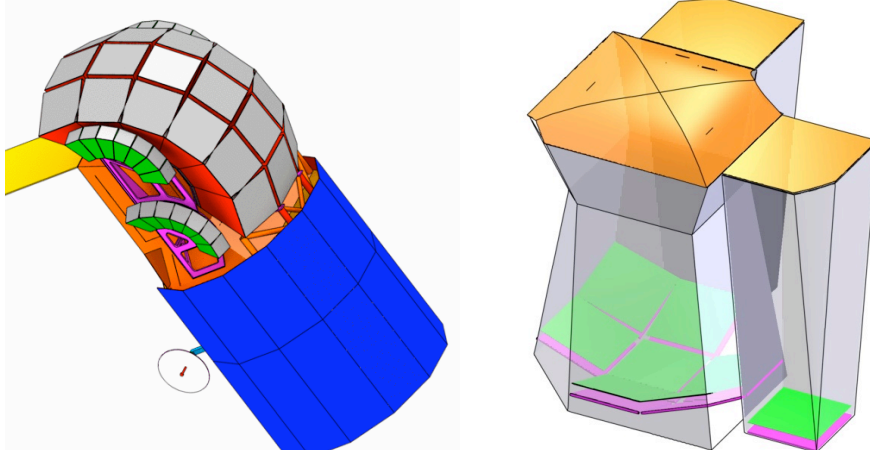


Figure 2. Two HET instrument concepts considered (a) Multiple sub-telescopes¹⁴ (b) A shared mask instrument (here the version considered in the 2008 Astrophysics Strategic Mission Concept Study, with two additional sub-telescopes).

different directions move in similar ways. The common motion is removed before the photons are binned. Two considerations limit the scan angle over which such corrections can be made: (i) at the limits of the detector plane, or where there are gaps in the detector plane such as those between sub-units in the EXIST detector array, photons are lost “off the edge” (ii) the tracks if the shadows from different sources are not exactly the same (see Fig. 3), nor are they traversed at exactly the same speed.

If the rotation is at an angular rate ω_x about an axis (x) normal to the instrument axis (z), the position in the detector of the shadow of a mask element at (x_m, y_m) cast by a source at an angle θ from the rotation axis and at an azimuth angle ϕ about the x -axis at time $t = 0$ is given by

$$x_d = x_m - \frac{f}{\tan \theta \cos(\omega_x t - \phi)} \quad (1)$$

$$y_d = y_m - f \tan(\omega_x t - \phi) \quad (2)$$

Thus for $t - t_0$ that is not too large, x_d is *approximately* constant and y_d is *approximately* proportional to time. But sources with a range of θ and ϕ_0 contribute to the flux received in a given part of the detector, so even after correction some blurring will remain. Using typical numbers for EXIST shows that errors can be kept below one detector pixel for sources up to 40° from the center of the field of view over integrations up to ~ 1 s. Without TDI the corresponding limit is 0.3 s for full resolution imaging (but see §5).

4. THE ON-BOARD PROCESSING PROBLEM

The numbers of ‘operations’ * for image reconstruction using brute force cross correlation is given by

$$N_{cc} \sim N_d N_s, \quad (3)$$

where N_d is the number of detector elements. For reconstruction by FFT it is

$$N_{FFT} \sim 2 N_{xy} \text{Log}_2(N_{xy}) \quad (4)$$

where

$$N_{xy} = [kN_d(x) + N_s(x) + B_x] \cdot [kN_d(y) + N_s(y) + B_y] \quad (5)$$

and where the maximum dimensions of the detector and sky arrays are $N_d(x) \times N_d(y)$ and $N_s(x) \times N_s(y)$. Here k is an oversampling factor because for the FFT to be used for the reconstruction the detectors pixels and the

*The term ‘operation’ here has different meanings in different cases but typically involves several look-ups, a mathematical operation and storing the results.

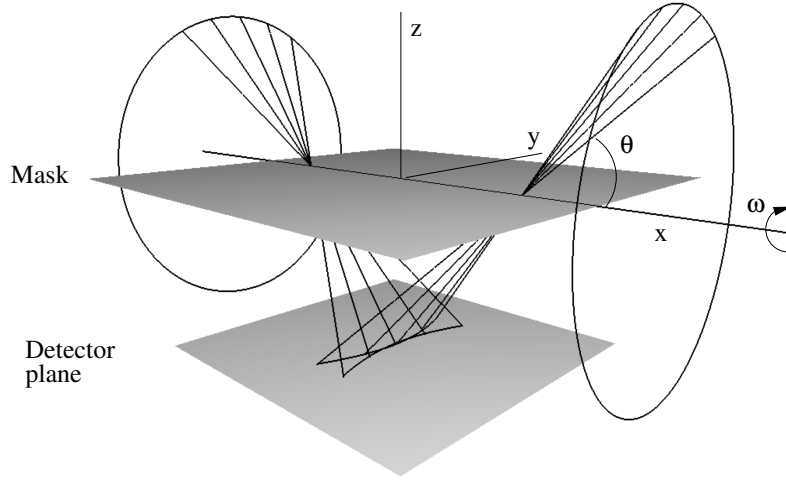


Figure 3. As the instrument scans, the track across the detector of the shadow of the mask depends on the direction of the source. Here for simplicity the scanning is assumed to be a simple rotation about an axis parallel to the mask. Sources in the two example directions indicated will appear to move in circles on the sky and so the tracks are parabolas formed where cones intersect the detector plane. They are traversed at non-uniform speed.

sky pixels must fall on a regular grids (in space coordinates and in tangent plane respectively) whose spacings are commensurate. Normally $k \geq 2$ for grids that are sufficiently fine that sources are not missed by being split between pixels. Finally B_x and B_y are the widths of border regions, padded with zeroes, introduced because the terms in square brackets must have simple factors – indeed Eqn. 4 supposes that they are powers of 2.

For image reconstruction by back-projection, the number of operations depends on the number of photons detected, N_p and the number of sky pixels, N_s for which a reconstruction is needed:

$$N_{bp} \sim N_p N_s. \quad (6)$$

The numbers given by equations 3 and 4 must be multiplied by the number of energy channels and divided by the integration time to give an indication of the number of operations per second needed. In contrast, provided enough memory is available, images can be reconstructed by back projection (Eqn. 6) in an arbitrary number of energy channels simultaneously and can be extracted on different timescales without penalty.

Table 1 gives an idea of the order of magnitude of the on-board computing task in terms of ‘operations’ per second. Processors that are space-qualified or currently being space-qualified have been identified that should make the FFT solution feasible, but the other solutions considered would require $\sim 10^3$ to 10^6 times more computing power. As noted above, the FFT solution demands a plane-parallel mask and detector.

Although image reconstruction by FFT appears marginally possible using the parameters in Table 1, there is relatively little margin, and anyway higher rates and more energy channels are desirable. For this reason a mask design allowing a two step approach has been adopted.

5. THE HYBRID MASK AND TWO-STAGE SOURCE LOCATION

The concept baselined for the EXIST HET involves a hybrid mask containing patterns on two spatial scales¹⁶ illustrated in Fig. 4. It has a large-scale (coarse) structure with a random pattern of elements on a 15 mm pitch, half of which are solid 3 mm thick tungsten. The ‘open’ elements of the coarse pattern contain thinner (0.3 mm) tungsten masks with random holes on a 1.25 mm pitch. Again 50% of the elements are solid[†]. The thickness of

[†]All of these dimensions and parameters are illustrative and may be subject to further optimization.

Table 1. Assumptions and the estimated size of the computing task.

Mask physical extent	$M_x \times M_y$	3380×2700	mm
Detector physical extent	$D_x \times D_y$	3380×1860	mm
Bin size	δ	0.6	mm
Corresponding angular scale*	δ/f	1	arc min
Number of sky pixels	$N_s = (M_x + D_x)(M_y + D_y)/\delta^2$	8.6×10^7	
Event rate	C	40000	events s ⁻¹
Number of actual detector pixels	N_d	1.2×10^7	
Number of energy channels	N_E	4	
Image rate	R	1	s ⁻¹
Padded array size for FFT	$N_{xy} = N_s$, rounded up to 2^n	$2^{27} = 134217728$	
‘operations’ per second			
Back projection	$N_{bp} = C N_s$	3.4×10^{12}	
Convolution (no FFT)	$N_{cc} = N_d N_s N_E R$	4.1×10^{15}	operations s ⁻¹
Convolution with FFT	$N_{FFT} = 2 N_{xy} \text{Log}_2 N_{xy}$	7.2×10^9	

*at center of FOV; reduced in proportion to $(1 + \sec^2 \theta)^{-1}$ at off-axis angle θ .

the coarse mask elements is chosen so that they are as opaque as possible over the entire operating energy range, while staying within mass constraints. The thin mask sections are designed to become largely transparent in the upper part of the energy range. The objectives of this design are to

1. ensure that both at low energies and at high the ‘open fraction’ of the mask is close to optimal (§5.1)
2. greatly reduce the computing power needed using a two step processing strategy (§5.2).

In addition, it

3. largely avoids an ‘auto-collimation’ problem – if holes as small as those in the fine mask sections (1.15 mm) were to be made in material thick enough to be largely opaque at high energies the field of view would be severely limited
4. reduces the number of events that have to be handled by the data processing and telemetry by having a low open fraction at low energies where the Cosmic X-ray background (CXB) dominates the counting rate, without loss of sensitivity except for very high time resolution studies of extremely bright sources.

5.1 Optimizing the open fraction

Fig. 5a shows that at energies below about 100 keV the detector background due to aperture-dependent effects (direct and indirect effects of the CXB) is expected to dominate over non-aperture-dependent background (particle-induced events, activation and indirect effects of penetrating high-energy gamma-rays). The fraction due to the former is shown as if there were no mask and in practice will be lower by a factor $\sim q$. In these circumstances $q < 50\%$ offers a sensitivity advantage, though in practice never a very large one.¹³ Fig. 5b shows the optimum q as a function of energy, together with the on-axis transmission t of the hybrid mask. At the lowest energies $t > q_{opt}$ because it becomes constant at $\sim 25\%$ (actually a little lower due to the supporting bars

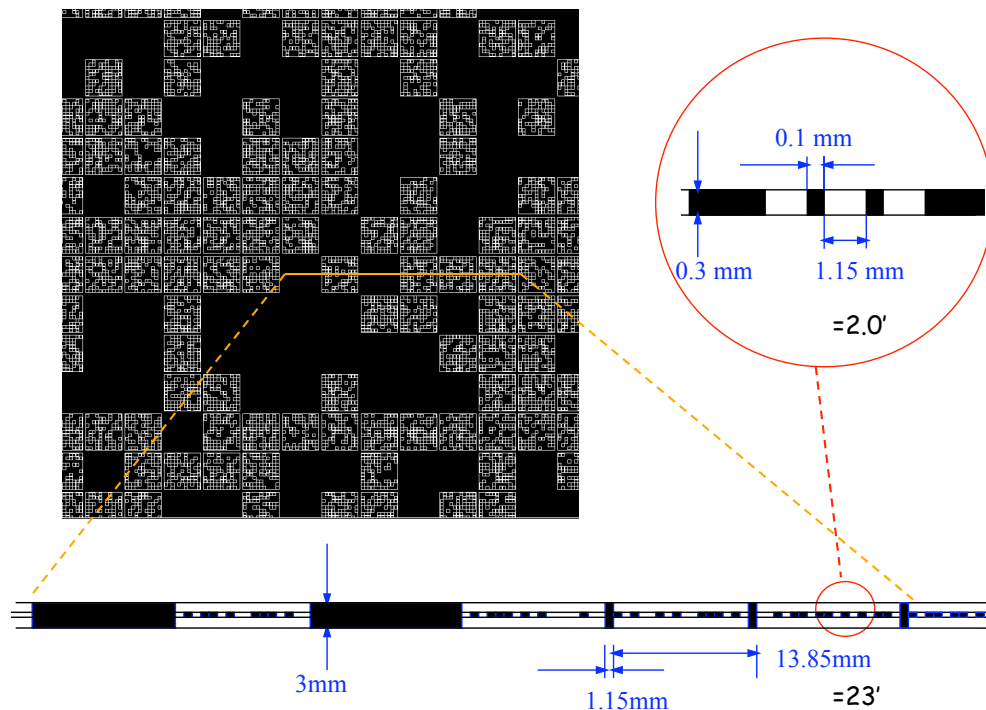


Figure 4. A small section of the hybrid mask proposed for the EXIST HET.

between elements). However it is always such as to give a sensitivity within 10% of that for q_{opt} . In fact the calculation of q_{opt} assumes that one is not limited by the number of source photons; for studying bright short bursts and QPOs there is an advantage in avoiding extremely low values of q . At the top end of the energy band it is again the case that $t > q_{opt}$. This arises because of leakage through the 3 mm thick coarse mask elements. The associated loss in sensitivity is inevitable given that mass limitations preclude making the elements thicker.

5.2 Imaging and source location

The most challenging objective of the HET on-board processing is the detection of GRBs and their localization as quickly as possible so that the satellite can be slewed to bring them within the fields of view of the other instruments. The principle and approach are very similar to those of Swift/BAT,^{17,18} but the size of the computing task is considerably greater. HET will have 1.2×10^7 detector pixels, compared to BAT's 32768 and the number of operations per FFT, N_{FFT} , is nearly 200 times larger. In addition, the objective is to obtain ~ 1 image per second whereas BAT requires 6 sec to form an image and on short timescales can only detect GRBs when a trigger has been first detected by monitoring event rates.

As well as providing near-optimal open fraction at all energies, the hybrid mask provides the key to reducing the burst detection processing problem to a manageable size. At low energies, even the 0.3 mm thin mask sections are effectively opaque. Viewed with the full resolution of the HET detector array, it therefore casts a shadow of the form in Fig. 6a. For high energy photons, the thin mask sections are largely transparent and only the coarse structure is seen (Fig. 6c). If the shadow is recorded with a coarsely binned detector – the fine mask regions become ‘gray’ and the shadow is predominantly that of the coarse mask, both at low energies and at high (Fig. 6b,d).

Consider what happens if an image is reconstructed using the coarsely binned detector data and an appropriately coarse representation of the mask pattern. The angular resolution will be approximately that corresponding to the coarse mask ($\sim 25'$), but there will be some loss of sensitivity because not all of the information potentially

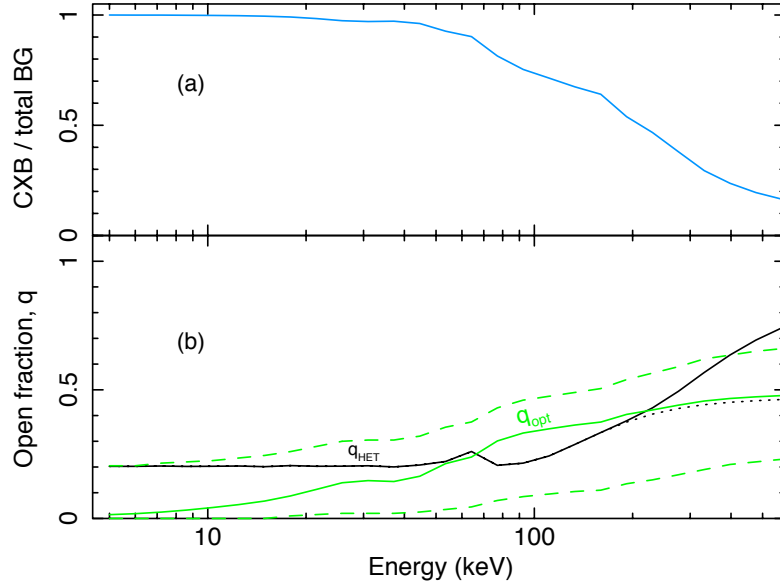


Figure 5. (a) The fraction of the total expected background in the HET due to aperture-dependent effects (e.g. CXB). The values given are for a fully open aperture (no mask, i.e. $q=1$). (b) The optimum value of the open fraction, q as a function of energy, based on the background estimates in (a). It is assumed that the noise is dominated by background, not by source counting statistics, which will generally be true for the HET. The dashed lines indicate the band within which the sensitivity is within 10% of that for the optimum q . Also shown is the transmission (on-axis) for the mask design in Fig. 4. The solid line is if leakage through the thick coarse mask elements is ignored; the dotted line shows the effect of including it.

available is being used. The effect on the sensitivity can be quantified using the ‘coding-power’. The coding power, Δ , of a mask-detector combination provides a measure of its sensitivity relative to a similar idealized configuration and in which the detector has the same background rate but with perfect spatial resolution and in which the mask has a pattern that is 50% perfectly open, 50% perfectly opaque[‡]. Δ is simply equal to twice the *rms* of mask transmission, as seen with the finite resolution detector (a number in the range 0–1). Fig. 7 shows how the sensitivity decreases as detector pixels are binned together, but also how the computing load decreases much faster.

The strategy proposed for detecting GRBs in the imaging mode involves, for each time and energy range combination, the following steps:

1. If the time range exceeds that for which TDI is possible, divide the data into sub-periods.
2. For each sub-period:
 - (a) Bin the data into coarse detector bins, correcting for mean shadow motion (ie TDI).
 - (b) Predict the response for each known bright source in the field of view; fit for the intensity of the source; subtract from the binned data array.
 - (c) Reconstruct a coarse image by FFT.
3. If there are multiple sub-periods overlay and combine the images on various timescales (*e.g.* 3, 10, 30 s ...)
4. Search the image for possibly significant points, using a low threshold ($N_{\sigma 1}$).

[‡]It is assumed that observation is limited by background and not by source flux or counting statistics (see Ref. 13).

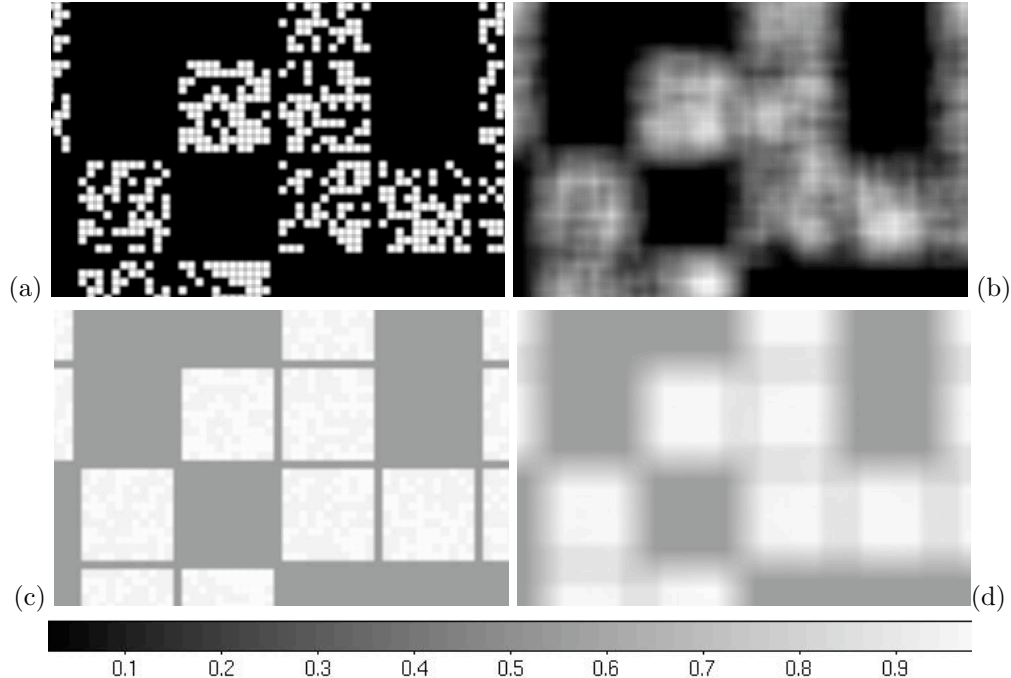


Figure 6. Part of the hybrid mask, seen at different energies and by a detectors with different spatial resolution. Top row (a,b): low energy (5keV). Bottom row (c,d): high energy (600 keV). Left (a,c): 0.6 mm detector resolution. Right (b,d): 6 mm resolution. The figures are convolutions of the shadow with a detector pixel; the actual response to the shadow cast by a point source would be this function, sampled on 0.6 or 6 mm grid.

5. For each possibly significant point, make full resolution local images around the location by back projection, using a detailed, energy-dependent, mask model and the actual spacecraft attitude at the time of arrival of the photon.
6. Optionally subtract a reference image.
7. Any peak greater than a higher threshold ($N_{\sigma 2}$) in one of these local images is considered a valid trigger.

The same procedure can be used for locating possible GRBs identified by monitoring event rates. In this case the energy band and time range will be those in which the rate increase was seen and the size of the field of view imaged initially in the coarse mask may be somewhat reduced if the candidate event was detected in a subset of the detector plane (e.g. a particular quadrant).

The strategy depends on the fact that although the coarse imaging is intrinsically less sensitive, by allowing a relatively large number of false triggers, a much lower threshold can be set. For a one-step analysis the threshold $N_{\sigma 1} = 6.9$ in Table 2 is chosen so that, taking into account the very large number of resolution elements in each image and the fact that one might be examining one image per second, the number of false triggers to which the spacecraft would slew is less than one per 2 days. On the other hand for the coarse imaging stage of a two-step analysis by allowing, say, 10 false triggers per coarse image, each of which will be followed-up by local fine-imaging using back-projection, the threshold can be reduced by nearly a factor of two – to $N_{\sigma 2} = 3.8$ for the figures in the table. The loss in sensitivity associated with coarse imaging is energy dependent (Fig. 7) but except at the lowest energies and the coarsest binning is less than the amount by which the threshold can be reduced. Thus any event detectable by full fine FFT imaging is almost certain to be detected by the two-step process with, in this example, about 40 times less computing load.

In practice a sort of two-step process could be adopted even with the fine FFT approach in that the location of a GRB would probably be found, and its significance confirmed, by follow-up back-projection in a small region

Table 2. Comparison of one-step and two-step strategies for detecting GRBs and transient sources. It is assumed that for the coarse imaging 10×10 detector pixels binned together and that typically 10 candidate peaks per coarse image are followed-up using detailed back-projection. Calculations are based on a single energy bin and one image per second.

	One-step	Two-step		Units
	Fine FFT	Coarse FFT	Fine back-projection	
Image size	5×10^8	5×10^6	1600	pixels
	2×10^7	2×10^6	100	resolution elements
Computation size	2×10^{10}	2×10^8	1.5×10^8	'operations'
Threshold	7.2	$N_{\sigma 1} = 3.9$	$N_{\sigma 2} = 7.2$	significance, σ
	1.0	$1.04^a - 0.83^b$	1.0	flux (relative)
False trigger rate ^c	3×10^{-13}	6×10^{-5}	3×10^{-13}	per resolution element
	6×10^{-6}	10	6×10^{-6}	per image
	0.5	(8×10^5)	0.5	per day

^a low energy ^b high energy ^c at given threshold.

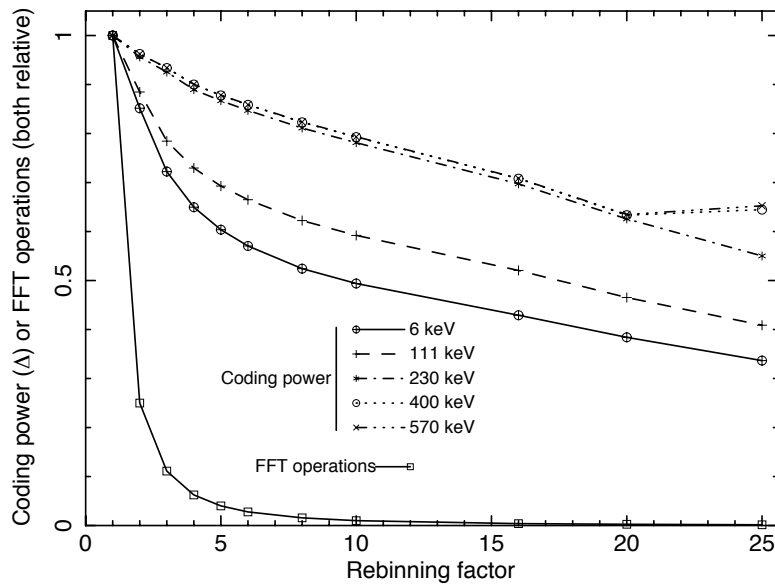


Figure 7. The effect of using coarsely binned data for image reduction. Coarse binning reduces the coding power (and hence sensitivity). The reduction is less at high energies, where the effective mask is predominantly the coarse one, than at low energy. The size of the computing task associated with an image reconstruction by FFT (square symbols, solid line) drops very rapidly.

around the peak. The threshold at the FFT stage could then be reduced somewhat and the higher one applied only after the follow-up. But this does not change any of the numbers in the Table except to increase slightly the already huge computational load associated with such an approach.

5.3 The Point Spread Function and source location accuracy

The Point Spread Function (PSF) is the normalized auto-correlation of the mask transmission convolved with the pixel footprint. With the hybrid mask the PSF is energy-dependent, as seen from the results of Monte Carlo

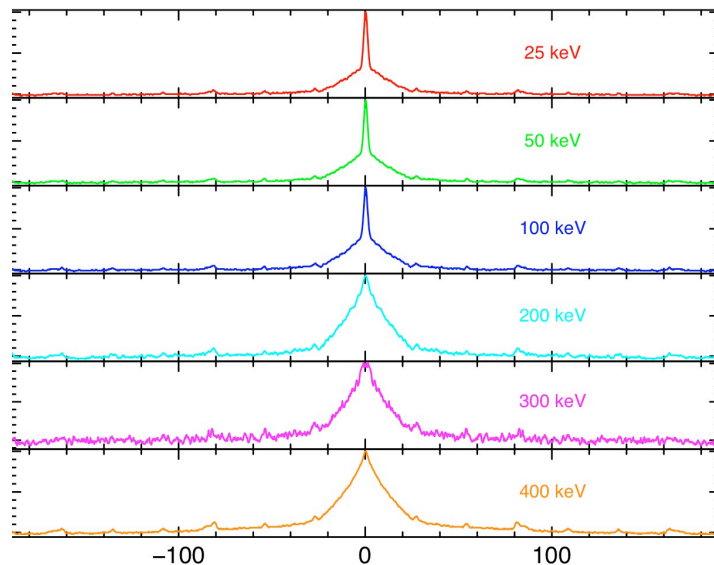


Figure 8. The PSF of HET with the hybrid mask, as a function of energy. The units are arc minutes.

simulations in Fig. 8. Together with the significance of detection, the PSF width sets a limit on the precision with which a source can be located. The 1σ source location accuracy for a source detected at significance N_σ is approximately the width of this function where it falls to a fraction $(1 - 1/N_\sigma)$ of the maximum. If N_σ is sufficiently large that a source is detected with confidence, then in practice this means that, except for the highest energies, it is the sharpness of the central spike that matters. That sharpness is inevitably inferior to that for a similar instrument with a (computationally impracticable) ‘fine-only’ mask, though the loss is alleviated by the fact that the detection will be at a slightly higher significance because the finite detector resolution has less impact.

6. SYSTEMATIC NOISE AND THE SKY SURVEY

The all-sky survey aspect of the EXIST objectives presents a different set of challenges. Data analysis will be in retrospect and on the ground, so computer power is much less of a constraint. The most important problem facing the mission design is then the minimization of systematic errors in order to obtain a sensitivity close to the theoretical limit when data from 2 years of observations are combined together. Systematic noise occurs in images reconstructed from coded-mask telescope data in two ways (a) imperfect modeling of the response to bright sources and hence residues left after their subtraction and (b) imperfect modeling of non-uniformities in the background. Spurious structure on a particular spatial scale, l , in the array representing the data in the detector plane leads to structure on the corresponding angular scale l/f in a reconstructed image. Thus when searching for point sources it is small scale residuals that are most important.

There is now considerable experience with deep hard X-ray surveys with the coded mask instruments INTEGRAL/IBIS and Swift/BAT. Of the two, Swift/BAT provides the closest analogy with EXIST/HET, though it has only $\sim 1/10$ the detector area and only 32000 detector pixels instead of more than 10^7 . BAT observations are divided into ‘snapshots’ of ~ 1000 s, with the same stable spacecraft attitude, after which there is a rapid slew to another attitude, though there may be a return to the first attitude, frequently one orbit later. Experience with Swift/BAT shows that near-Poisson-noise limited sensitivity can be achieved in single snapshots, but that extreme care is necessary when combining together images from multiple snapshots, particularly when the spacecraft attitudes are similar.

EXIST will have two major advantages over INTEGRAL and Swift in the battle against systematic noise. First, the much greater number of detector pixels helps. To the extent that the contributions from different

detector pixels to the systematic noise are uncorrelated in sky coordinates, there is an advantage that goes with the square-root of the number of pixels – a factor of ~ 20 . Secondly the EXIST HET will take an effectively different snapshot every ~ 0.5 s, compared with ~ 1000 s for BAT. Again assuming that the noise in sky coordinates is uncorrelated, this implies a further reduction in systematic noise by a factor >40 . Another way of looking at the problem is to note that during a 2 year survey, as a result of the scanning, each of the 1.2×10^7 detector pixel will acquire $\sim 10^9$ measurements in each energy band.

7. CONCLUSIONS

EXIST is an ambitious mission that will detect GRBs more distant than any studied to date and up to an order of magnitude fainter. The challenges that it presents in terms of on-board detection and location of transient events and of the reduction of systematic noise can be overcome only because of the adoption of a simple geometry that makes correlation efficient and a mask design that permits a two-step detection and location of new sources.

ACKNOWLEDGMENTS

The EXIST mission studies involve a very large number of people. The authors are members of the EXIST HET Imaging Technical Working Group. We gratefully acknowledge the efforts of the other contributors to this large community effort. Partial support for this study was derived from NASA-ASMC grant NNG04GK33G.

REFERENCES

1. Grindlay, J., “GRB Probes of the High-z Universe with EXIST,” *AIP Conference Series* **1133**, 18–24 (2009).
2. Bloom, J. S., Holz, D. E., Hughes, S. A., and Menou, K., “Coordinated Science in the Gravitational and Electromagnetic Skies,” *Astro2010: The Astronomy and Astrophysics Decadal Survey, Science White Papers* **20** (2009).
3. McQuinn, M. et al., “In Situ Probes of the First Galaxies and Reionization: Gamma-ray Bursts,” *Astro2010: The Astronomy and Astrophysics Decadal Survey, Science White Papers* **199** (2009).
4. Grindlay, J. et al., “Measuring the Accreting Stellar and Intermediate Mass Black Hole Populations in the Galaxy and Local Group,” *Astro2010: The Astronomy and Astrophysics Decadal Survey, Science White Papers* **105** (2009).
5. Soderberg, A. et al., “The Dynamic X-ray Sky of the Local Universe,” *Astro2010: The Astronomy and Astrophysics Decadal Survey, Science White Papers* **278** (2009).
6. Coppi, P. et al., “Lifting the Veil on the Black Hole-Galaxy Connection: Opportunities for 2010-2020,” *Astro2010: The Astronomy and Astrophysics Decadal Survey, Science White Papers* **55** (2009).
7. Hong, J. S. et al., “The High Energy Telescope (HET) on EXIST,” *These proceedings* **7435** (2009).
8. Tagliaferri, G., A. S. et al., “SXI on board EXIST: scientific performances,” *These proceedings* **7435** (2009).
9. Kutuyev, A. S. et al., “EXIST IRT imager-spectrometer,” *These proceedings* **7453** (2009).
10. Fenimore, E. E., “Time-resolved and energy-resolved coded aperture images with URA tagging,” *Appl. Opt.* **26**, 2760–2769 (1987).
11. Bird, A. J. and Merrifield, M. R., “X-ray all-sky monitoring and transient detection using a coded sphere telescope,” *Astron. & Astrophys. Supp.* **117**, 131–136 (1996).
12. Skinner, G. K., “Coding (and Decoding) Coded Mask Telescopes,” *Experimental Astronomy* **6**, 1–7 (1995).
13. Skinner, G. K., “Sensitivity of coded mask telescopes,” *Appl. Opt.* **47**, 2739–2749 (2008).
14. Grindlay, J. E., “EXIST: All-sky hard X-ray imaging and spectral-temporal survey for black holes [review article],” *New Astronomy Review* **49**, 436–439 (2005).
15. Copete, A. et al. *Papers in preparation* (2009).
16. Skinner, G. K. and Grindlay, J. E., “Coded masks with two spatial scales,” *Astron. & Astrophys.* **276**, 673 (1993).
17. Barthelmy, S. D. et al., “The Burst Alert Telescope (BAT) on the SWIFT Midex Mission,” *Space Science Reviews* **120**, 143–164 (2005).
18. Palmer, D. M. et al., “The BAT-Swift Science Software,” *AIP Conference Series* **727**, 663–666 (2004).